Design and Forward Kinematics of the Compliant Micro-manipulator with Lever Mechanism

Y. Tian[1,2], B. Shirinzadeh[1], D. Zhang[2], X. Liu[3], D. Chetwynd[3]

[1]Robotics & Mechatronics Research Laboratory, Department of Mechanical and Aerospace Engineering, Monash University, Clayton, VIC 3800, Australia

[2]School of Mechanical Engineering, Tianjin University, Tianjin 300072, China

[3]School of Engineering, University of Warwick, Coventry CV4 7AL, UK

Abstract: This paper presents the forward kinematics of a five-bar compliant micro-manipulator, which is indispensable for the applications of micro/nano scale operations. To overcome the limited displacement of such a flexure-based mechanism and its piezoelectric actuators, lever mechanisms are used to enlarge the working range in Cartesian space. The mechanical design of the micro-manipulator is firstly described. Based on the configuration of the proposed flexure-based micro-manipulator, the entire system has been divided into a five-bar mechanism and two four-bar amplification mechanisms. For the five-bar mechanism, two mathematical expressions describing the path traced by the tips of two passive links connected to each other are obtained. The solution is developed to determine the Cartesian coordinates of the connection points for the passive links. Thus, the Cartesian coordinates of the end-effector attached to one of the passive links is obtained according to the established geometric relationship. The amplification factor of the lever mechanism is also derived based on the analytical solution of the four-bar linkage. The velocity of the end-effector is obtained by differentiating the forward position kinematic equation, and the local mobility index of the five-bar compliant mechanism is determined and analyzed. Based on the simplification methodologies such as linearising the

trigonometric functions and constant Jacobian matrix, numerical simulations have been carried out to investigate the performance of the five-bar compliant manipulator and to determine the optimal geometric parameters for the configuration. The comparisons between the exact solution and simplified methodologies are carried out. It is noted that the linearising trigonometric simplification has a higher accuracy and is more suitable for the kinematic calculation of the micro-manipulator, but the constant Jacobian matrix method can efficiently calculate the forward kinematics of the micro-manipulator with the acceptable accuracy, which is important for real-time control system. Experimental tests are carried out to validate the established model and the performance of the developed micro-manipulator.

Keywords: micro-manipulator, flexure hinge, forward kinematics, mechanical design

1. Introduction

Micro/nano manipulation is one of the key techniques for the nanotechnology applications such as x-ray lithography, micro-manufacturing, biomedicine, micro-surgery, and nano-metrology [1-5]. In these engineering fields, the required motion and positioning precision is generally within the order of magnitude of nanometer. It is well known that the positioning precision and resolution of the micro-manipulators mainly depend on the topology and mechanical structure, actuator and transducer, sensing and measurement, and control methodologies [6]. In order to improve the positioning accuracy of conventional robotic manipulators, a laser-based interferometry sensing and measurement technique, which has the advantages including high accuracy, large workspace, high sampling rate and dynamic target tracking, has firstly been utilized to measure the displacement of the manipulators for

the purpose of the stiffness modeling, kinematic calibration and error compensation [7, 8]. Furthermore, the uncertainties in the laser-based interferometry sensing and measurement technique have also been systematically investigated to improve the robustness, stability and precision of the measurement [9]. Recently, the laser-based interferometry guide technique has been proposed to improve the positioning accuracy of the manipulator, where the laser-based interferometry sensing and measurement apparatus is utilized as displacement sensor for obtaining the position of the end-effector to form the closed-loop control [10, 11]. Although these methodologies can improve the positioning precision of the manipulator to some extent, it is impossible to make the conventional manipulator to fulfill the requirements of the micro/nano manipulation tasks.

The main reasons that prevent the conventional manipulator from improvement of the positioning accuracy are mainly due to the backlash and stiction of the revolute joints and the geometric and dimensional errors of the components of the manipulator [12]. These also stop the conventional mechanisms using laser-based measurement and control technique to be utilized as micro-manipulators. Therefore, different manipulators must be developed that can overcome these problems. One of the best choices to overcome the problems is using flexure-based compliant mechanism, where the conventional kinematic pairs are replaced by the flexure hinges. These types of the joints have a number of advantages including no backlash, zero friction, and negligible hysteresis [13-16]. In addition, such a flexure-based micro-manipulator can be monolithically manufactured, and thus reduce assembly errors and guarantee the machining accuracy [17]. Furthermore, the flexure-based micro-manipulator can be combined with the conventional macro-positioning manipulators to form the dual

positioning system. Thus, the large range of precision positioning can be achieved [18, 19]. Research efforts have focused on the development of many aspects of the micro-manipulators for conducting nano-scale tasks beyond the limits of human manipulation and patience [20-23]. The development of these design methodologies for the flexure hinge, novel micro-actuators, and adaptive robust control strategies for precision positioning will help facilitate the micro-manipulator with high dynamic performance and resolution [24-27]. It is known that the piezoelectric parallel-actuated closed-loop mechanisms made up of flexure hinges have demonstrated a considerable potential for the applications in the micro-manipulation tasks [28, 29]. The forward kinematics is one of the important research areas in the applications of the parallel micro-manipulator.

This paper presents the forward kinematics for the Cartesian displacement and velocity of a flexure-based micro-manipulator. The design methodology of the micro-manipulator with lever mechanisms is described. The strategy for the choice of the end-effector on the links of the five-bar mechanism is presented, and the prototype of the flexure-based five-bar micro-manipulator is developed based on the proposed design methodology. The forward kinematics of the five-bar mechanism is obtained by solving the intersection points of two circles whose centers locate at the end of the active links and radii equal to the lengths of the passive links, respectively. The amplification factor of the lever mechanism is also achieved by considering the amplification mechanism as a special four-bar linkage. The velocity of the end-effector of the five-bar mechanism is obtained by differentiating the forward position kinematic equation, and thus the local mobility index of the five-bar compliant mechanism is provided. Based on the simplification methodologies such as linearising trigonometric

functions and constant Jacobian matrix, numerical simulations have been carried out and calculation precision of the simplified methodologies is presented.

2. Mechanical Design

The 3D model of the five-bar compliant micro-manipulator with lever mechanisms is shown in Fig.1. The main components of the compliant mechanism include the rectangular links and flexure hinges. Compared with other types of flexure hinges, circular flexure hinge with rectangular cross-section has high precision for rotational accuracy and is the optimal choice as the revolute joint for precision mechanism design and construction. A stationary frame is used to support the compliant mechanism and connect with other equipment.

The five-bar linkage, demonstrated as loop 1, is the main mechanism to implement 2-DOF (degree of freedom) planar motion. The location of the end-effector is one of the key factors to affect the kinematic and dynamic characteristics of the compliant mechanism. The end-effector should be located at the mid-point of the central flexure hinge, and thus the entire mechanism has a symmetric kinematic and dynamic performance within the Cartesian space. However, it is not feasible for the end-effector to be located at the mid-point of flexure hinge to implement micro-manipulation or mount other tools and measurement sensors for closed-loop control. The main reason is that flexure hinge will generate elastic deformation during the motion of the five-bar mechanism, and the position and orientation of the mid-point of the flexure hinge are difficult to model and predict, and thus the positioning precision of the end-effector is seriously affected.

To overcome the above problem, the end-effector is chosen at the location on one of the

passive links as shown in Fig.1. Due to no local elastic deformation, the position and orientation of the end-effector can be accurately predicted and controlled, the feedback measurement sensors can also be mounted onto the end-effector to form the closed-loop control and improve the static and dynamic performance of the five-bar micro-manipulator. Furthermore, the kinematic performance of the end-effect within the Cartesian space can be improved by optimization of the structural parameters such as the link lengths and the initial angles of the five-bar mechanism. Thus, the end-effector of the five-bar mechanism can also achieve an approximately symmetric kinematic performance within the Cartesian space.

It is well known that the performance of the actuator significantly affects the static and dynamic characteristics of the compliant mechanism. Piezoelectric actuator is generally utilized to drive flexure-based mechanism, due to the advantages such as infinite resolution, zero backlash, no lubrication, and free of thermal generation. Whereas, the limited output displacement is the disadvantage of this kind of actuator. In order to obtain the required working range, a lever mechanism may be utilized to enlarge the displacement of the piezoelectric actuator as shown in Fig. 1, where two lever mechanisms are designed to drive the active links of the five-bar mechanism.

The prototype of the five-bar micro-manipulator has been developed and shown in Fig. 2, where the entire mechanism is monolithically manufactured by use of WEDM (wire electro-discharge machining) technique, and the geometric size and tolerance of the links and flexure hinges are strictly controlled to guarantee the motion accuracy. The material for the compliant mechanism is chosen as the aluminum alloy T7075, which has high performance and stability and is suitable for the flexure-based micro-manipulator design and construction.

3. Kinematic Modeling

From the kinematic point of view, a rectangular circular flexure hinge can generate rotation about one axis, and is simplified as an ideal revolute joint. This indicates that the drift of the center of rotation during the motion of the relative links is not taken into consideration. During the kinematic analysis, the stiffness of the flexure hinges is also neglected. Furthermore, the deformation of the links due to the bending moment can be negligible through the optimal mechanical design. Thus, the kinematic model of the five-bar mechanism is obtained and shown in Fig.3, where *OA* and *DB* are the active links, *AP* and *BP* are the passive links, and *PM* is the extended part of the passive link *AP*. The active links *OA* and *DB* have the initial angular positions of θ_1 and θ_2 from the positive direction of the *x* axis. The length of the links is r_i (i=0, 1, ···, 5), and the angle α is the angle of link *PM* separating from link *AP*. Based on the geometric and motion relationships, the following equations can be given:

$$\boldsymbol{r}_1 = r_1 \cos\theta_1 i + r_1 \sin\theta_1 j \tag{1}$$

$$\boldsymbol{r}_6 = (r_0 + r_5 \cos\theta_2) i + r_5 \sin\theta_2 j \tag{2}$$

$$\boldsymbol{q} = \boldsymbol{r}_6 - \boldsymbol{r}_1 = Ci + Dj \tag{3}$$

where $C = r_0 + r_5 \cos\theta_2 - r_1 \cos\theta_1$, $D = r_5 \sin\theta_2 - r_1 \sin\theta_1$.

The coordinates of the point *P* can be determined by the intersection of two circles whose centers locate at the points *A* and *B*, and the radii of the two circles are r_2 and r_4, respectively. It must be mentioned that the locations of the points *A* and *B* are the functions of the input angles θ_1 and θ_2. The two intersections are the possible solution for the point *P*. Based on the

specified link lengths and driving angles, the coordinates of points $P_1(x, y)$ and $P_2(x, y)$ are given as follows:

$$\begin{cases} x_{P1} = r_1 \cos\theta_1 + r_2 (QC - DE) \\ y_{P1} = r_1 \sin\theta_1 + r_2 (QD + CE) \end{cases} \tag{4}$$

and

$$\begin{cases} x_{P2} = r_1 \cos\theta_1 + r_2 (QC + DE) \\ y_{P2} = r_1 \sin\theta_1 + r_2 (QD - CE) \end{cases} \tag{5}$$

where $Q = \dfrac{r_2^2 + q^2 - r_4^2}{2 r_2 q^2}$, $E = \sqrt{1/q^2 - Q^2}$.

Thus, the possible locations of point $M(x, y)$ can be given as follows:

$$\begin{cases} x_{M1} = x_{P1} + r_3 \cos\alpha (QC - DE) - r_3 \sin\alpha (QD + CE) \\ y_{M1} = y_{P1} + r_3 \cos\alpha (QD + CE) + r_3 \sin\alpha (QC - DE) \end{cases} \tag{6}$$

and

$$\begin{cases} x_{M2} = x_{P2} + r_3 \cos\alpha (QC + DE) - r_3 \sin\alpha (QD - CE) \\ y_{M2} = y_{P2} + r_3 \cos\alpha (QD - CE) + r_3 \sin\alpha (QC + DE) \end{cases} \tag{7}$$

Based on the geometric relationship, Eq. (6) is chosen as the forward kinematics of the five-bar mechanism.

Assume that the links $OA = DB$, $AP = BP$, respectively, -i.e. $r_1 = r_5$ and $r_2 = r_4$. For the brevity and without loss of generality, two vectors $\boldsymbol{\Gamma} = (x_M, y_M)^{\mathrm{T}}$ and $\boldsymbol{\Theta} = (\theta_1, \theta_2)^{\mathrm{T}}$ are introduced.

By differentiating Eq. (6) with respect to time, the following relationship may be written:

$$\dot{\boldsymbol{\Gamma}} = \begin{bmatrix} \dfrac{\partial x_M}{\partial(\theta_1, \theta_2)} \\ \dfrac{\partial y_M}{\partial(\theta_1, \theta_2)} \end{bmatrix} \dot{\boldsymbol{\Theta}} = \boldsymbol{J}\dot{\boldsymbol{\Theta}} \tag{8}$$

where $\boldsymbol{J} = \begin{bmatrix} J_{11} & J_{12} \\ J_{21} & J_{22} \end{bmatrix}$ is the Jacobian matrix and defined by:

$$J_{11} = -r_1 \sin\theta_1 + r_1\left(r_2 + r_3\cos\alpha\right)\left[\frac{\sin\theta_1}{2r_2} + E\cos\theta_1 + \frac{D}{q^4 E}\left(C\sin\theta_1 - D\cos\theta_1\right)\right]$$
$$- r_1 r_3 \sin\alpha\left[-\frac{\cos\theta_1}{2r_2} + E\sin\theta_1 - \frac{C}{q^4 E}\left(C\sin\theta_1 - D\cos\theta_1\right)\right]$$

$$J_{12} = r_1\left(r_2 + r_3\cos\alpha\right)\left[-\frac{\sin\theta_2}{2r_2} - E\cos\theta_2 + \frac{D}{q^4 E}\left(-C\sin\theta_2 + D\cos\theta_2\right)\right]$$
$$- r_1 r_3 \sin\alpha\left[\frac{\cos\theta_2}{2r_2} - E\sin\theta_2 - \frac{C}{q^4 E}\left(-C\sin\theta_2 + D\cos\theta_2\right)\right]$$

$$J_{21} = r_1\cos\theta_1 + r_1\left(r_2 + r_3\cos\alpha\right)\left[-\frac{\cos\theta_1}{2r_2} + E\sin\theta_1 - \frac{C}{q^4 E}\left(C\sin\theta_1 - D\cos\theta_1\right)\right]$$
$$+ r_1 r_3 \sin\alpha\left[\frac{\sin\theta_1}{2r_2} + E\cos\theta_1 + \frac{D}{q^4 E}\left(C\sin\theta_1 - D\cos\theta_1\right)\right]$$

$$J_{22} = r_1\left(r_2 + r_3\cos\alpha\right)\left[\frac{\cos\theta_2}{2r_2} - E\sin\theta_2 - \frac{C}{q^4 E}\left(-C\sin\theta_2 + D\cos\theta_2\right)\right]$$
$$+ r_1 r_3 \sin\alpha\left[-\frac{\sin\theta_2}{2r_2} - E\cos\theta_2 + \frac{D}{q^4 E}\left(-C\sin\theta_2 + D\cos\theta_2\right)\right]$$

The generalized Jacobian matrix, $\boldsymbol{J}_{\mathrm{G}}$, defined as the quadratic form of the Jacobian matrix $\boldsymbol{J}$, is used to characterize the force manipulability of the mechanism. $\boldsymbol{J}_{\mathrm{G}}$ can be written as the product of two matrices:

$$\boldsymbol{J}_{\mathrm{G}} = \boldsymbol{J}\boldsymbol{J}^{\mathrm{T}} \tag{9}$$

The propagation from the input joint torques to the output end-effector force is directly proportional to the eigenvalues of $\boldsymbol{J}_{\mathrm{G}}$. If the eigenvalues of the generalized Jacobian matrix are $\sigma_{\max}$ and $\sigma_{\min}$, it is acknowledged that when the end-effector force is in the direction of

eigenvector e_{max} related to the maximum eigenvalue of $\boldsymbol{J}_G$, the largest joint torque is required to exert a unit Cartesian force. Thus, the force manipulability at the end-effector of the mechanism is at the worst condition. On the other hand, the force manipulability is at its best condition when a force is exerted in the direction of eigenvector e_{min}. The local mobility index k is defined as the ratio between the maximum and minimum eigenvalues of the generalized Jacobian matrix, $\boldsymbol{J}_G$, which is also called the condition number of the Jacobian matrix $\boldsymbol{J}$ and defined by:

$$k = \frac{\sigma_{max}}{\sigma_{min}} \tag{10}$$

The lever mechanism (loop 2 shown in Fig.1) can be considered as a four-bar mechanism and illustrated in Fig.4, where the length of the links is l_i (i=0, 1, 2, 3), and θ_i (i=3, 4, 5) is the angle of the links with respect to the positive direction of x' axis. Thus, the four links form a closed-loop equation and the projection on x' and y' axes are given, respectively:

$$l_1 \cos\theta_3 + l_2 \cos\theta_4 - l_3 \cos\theta_5 - l_0 = 0 \tag{11}$$

$$l_1 \sin\theta_3 + l_2 \sin\theta_4 - l_3 \sin\theta_5 = 0 \tag{12}$$

Substituting Eq. (11) into Eq. (12), and eliminating θ_4, yields:

$$f = \left(l_1 \cos\theta_3 - l_3 \cos\theta_5 - l_0\right)^2 + \left(l_1 \sin\theta_3 - l_3 \sin\theta_5\right)^2 - l_2^2 = 0 \tag{13}$$

Thus, the relation between θ_3 and θ_5 can be derived as follows:

$$\frac{d\theta_5}{d\theta_3} = -\frac{\partial f/\partial\theta_3}{\partial f/\partial\theta_5} = -\frac{l_1\left(l_3 \sin(\theta_3 - \theta_5) + l_0 \sin\theta_3\right)}{l_3\left(l_1 \sin(\theta_5 - \theta_3) - l_0 \sin\theta_5\right)} \tag{14}$$

When link l_1 is parallel to link l_3, - i.e. $\theta_3 - \theta_5 = \pi$, Eq. (14) can be simplified and rewritten as:

$$d\theta_5 = -\frac{l_1}{l_3} d\theta_3 \tag{15}$$

It is noted that the amplification factor of the lever mechanism is proportional to the ratio of the links l_1 and l_3, when the mechanism moves within a small range. In addition, the link l_2 should be perpendicular to the links l_1 and l_3, in order to obtain a large transmission angle.

The exact solution of the forward kinematics of the five-bar mechanism can be carried out based on the Eq. (6). In order to improve calculation efficiency, the solution of the forward position problem has been implemented by two simplified methods: (a) linearising the trigonometric functions for small displacement in Eq. (6), and (b) approximating the velocity equation, in Eq. (8), for small displacement equation in the actuation and Cartesian spaces. Thus, the small displacement mapping between the actuation and Cartesian spaces can be given as follows:

$$\begin{bmatrix} \delta x \\ \delta y \end{bmatrix} = \boldsymbol{J} \begin{bmatrix} \delta\theta_1 \\ \delta\theta_2 \end{bmatrix} \tag{16}$$

where δx and δy are the small displacement of the end-effector in the Cartesian space, $\delta\theta_1$ and $\delta\theta_2$ are the small displacement of the active links in the actuation space.

The similar method can be used to determine the velocity of the five-bar manipulator in Cartesian space to improve the calculation efficiency. The first approach is based on the linearising all the trigonometric functions in Eq. (8). The second method uses a constant Jacobian matrix through the range of motion while evaluating the Cartesian velocity vector.

4. Numerical Results and Discussion

Under the special configuration of the lever mechanism, -i.e. the active link l_1 is parallel with the link l_3 of the five-bar mechanism as shown in Fig.4, the amplification factor of the lever mechanism is constant and equal to the length ratio of the two corresponding links. Thus, the kinematic and dynamic characteristics of the compliant mechanism are determined by the configuration of the five-bar mechanism. Assuming that the link lengths for the five-bar mechanism are r_0=147 mm, r_1=r_5=58.458 mm, r_2=r_4=53.68 mm, and r_3=8 or 16 mm, the local mobility indices of the five-bar mechanism with different end-effector position are shown in Fig.5, where the initial angles for the active links are chosen as θ_1= 1.0421 rad and θ_2= 2.0995 rad. From the initial position, the active links are commanded to move within the displacement of $\delta\theta_1$= $\delta\theta_2$= $\pm\pi/6$ rad with the step size s=0.005 rad. From the simulation results, it can be seen that the five-bar mechanism has a symmetric local mobility index when the point *P* is chosen as the end-effector. Whereas, it is not practicable to choose point *P* as the end-effector, due to the local deformation introducing uncertainty of the position and orientation. Thus, the alternative point *M* attached to the passive link 2 is chosen as the end-effector. It is noted that the local mobility index of the point *M* is asymmetric within the working space, and the value of the local mobility index of the point *M* is larger than that of the point *P*. The value of the mobility index of the point *M* will increase with the increment of link length r_3 and angle α. This indicates that the larger joint torque is needed to drive the unit load in Cartesian space when the point *M* is the end-effector. In addition, the asymmetry of the local mobility index also increases with the increase of the link length r_3 and angle α, and this is harmful for the closed-loop controller design and performance improvement of the five-bar mechanism. In order to guarantee the static and dynamic characteristics of the entire

compliant mechanism, the end-effector point M should be chosen as close as possible to the point P. This is useful to achieve the required performance of the micro-manipulator.

With the consideration of the local mobility index in mind and directing on attention to the feasibility of the configuration, the position of the point M is chosen as: the link length r_3=8 mm, α=1.8155 rad, and the initial position of the active links are chosen as θ_1= 1.0421 rad and θ_2= 2.0995 rad. The strokes of the active links are set as $\delta\theta_1 = \delta\theta_2 = \pm 20\times10^{-6}$ rad with a step s=0.5×10^{-6} rad. The angular velocities of the active links are chosen as $\dot{\theta}_1 = \dot{\theta}_2 = 1\times10^{-4}$ rad/s. Thus, the position and velocity of the points P and M are determined using the developed forward kinematic formulations and the simplified methodologies described in the previous section.

The position errors of the points P and M in x and y directions corresponding to four different simplified forward kinematic solutions are provided in Figs. 6 and 7, respectively. The linearised function plots (Figs. 6a and 7a) show the position errors between the exact position solutions and the simplified solutions with linearised sine and cosine functions in the forward kinematic equations. It is noted that the error contours are the lines with almost the same slope, and the position errors are negligibly small. The position errors of the point P in the x and y direction are within the bands of $\delta x \approx 1.3\times10^{-11}$ m and $\delta y \approx 1.5\times10^{-11}$ m, and those of the point M in the x and y directions are located in the ranges of $\delta x \approx 1.7\times10^{-11}$ m and $\delta y \approx 1.8\times 10^{-11}$ m. In addition, the error contours of the point P are symmetric and those of point M are asymmetric. When Eq. (16) is used to evaluate the position of the end-effector, the position errors of the point P (Fig. 6b) in x and y directions increase to the ranges of $\delta x \approx 3.0\times10^{-11}$ m and $\delta y \approx 5.5\times10^{-11}$ m, and those of the point M (Fig. 7b) reach up to the bands of

$\delta x \approx 3.4\times10^{-11}$ m and $\delta y \approx 6.2\times10^{-11}$ m in the x and y directions, respectively. Furthermore, the position errors in y direction of the points P and M become asymmetric. When the trigonometric functions of the Jacobian matrix are linearised, the error contours of the points P and M (Figs. 6c and 7c) are the same as the solutions based on the exact Jacobian matrix. When the constant Jacobian matrix for the configuration of $\theta_1 = \pi/3$ rad and $\theta_2 = 2\pi/3$ rad is utilized to calculate the forward position of the five-bar compliant mechanism (Figs. 6d and 7d), the magnitude of values of position errors for the points P and M, are similar to those of exact or linearised Jacobian matrix, but the signs of the errors are opposite. From the computational results, it can be concluded that the linearising trigonometric functions in forward kinematic equation obtains the higher order of the magnitude precision for position prediction. The forward kinematic solution using simplified methods such as linearised and constant Jacobian matrix can be obtained with the similar precision for forward position prediction. Those simplified methods have the same order of magnitude for the precision of prediction. In addition, the constant Jacobian matrix corresponding to any configuration of the manipulator within the specified ranges of θ_1 and θ_2 can be used to calculate the forward kinematic position prediction, and the error ranges will not change significantly. This conclusion is in agreement with the research results [22, 30], and it is important and useful for the forward kinematic calculation of the parallel micro-manipulators. It is also noted that the simplified methods can induce larger position errors at the point M. Thus, the point M should be chosen as close as possible to the point P. This conclusion is similar to that drawn from the local mobility index consideration.

The velocity errors in x and y directions of the points P and M are shown in Figs. 8 and 9. It

is noted that the error contours are also the lines with almost the same slope, during the angles of the active links change within the ranges of $\theta_1+\delta\theta_1$ and $\theta_2+\delta\theta_2$. When the trigonometric functions of Jacobian matrix are linearised to calculate the Cartesian velocity of the end-effector, the velocity errors of the point P in the x and y directions locate within the ranges of $\delta\dot{x} \approx 3.2\times10^{-16}$ m/s and $\delta\dot{y} \approx 2.2\times10^{-15}$ m/s, respectively. Similarly, the velocity errors of the point M in the x and y directions stay within the ranges of $\delta\dot{x} \approx 5.8\times10^{-16}$ m/s and $\delta\dot{y} \approx 2.5\times10^{-15}$ m/s, respectively. When the constant Jacobian matrix is utilized to calculate the velocity of the end-effector, the velocity errors of the point P dramatically increase to the ranges of $\delta\dot{x} \approx 6.0\times10^{-10}$ m/s and $\delta\dot{y} \approx 5.0\times10^{-10}$ m/s. The velocity errors of the point M will reach up to the ranges of $\delta\dot{x} \approx 6.8\times10^{-10}$ m/s and $\delta\dot{y} \approx 5.6\times10^{-10}$ m/s. Although the constant Jacobian matrix can induce larger prediction errors than the linearised Jacobian matrix, the computational errors are very smaller compared to the absolute velocity of the end effector. Thus, the constant Jacobian matrix can be used to calculate the velocity of the end-effector with an acceptable precision and high computational efficiency, and this is important for the realization of real-time control algorithm.

5. Experimental tests

In order to examine the performance of the developed flexure-based five-bar mechanism, a number of experimental tests have been carried out. A Newport optical table is used to reduce the effects of the external disturbance on the measure and sensing system, and a high precision displacement sensor is utilized to measure the output of the flexure-based

mechanism. Fig.10 shows the displacement characteristics of the piezoelectric actuators under the free and assembling conditions. The open-loop and closed-loop performance is provided to demonstrate the hysteresis of the piezoelectric ceramics. It is noted that there is large difference between the expansion and retraction processes under open-loop control condition. These non-linear phenomena can be eliminated by use of closed-loop control method. Due to the stiffness effect of the flexure mechanism, the actual displacement of the driving points is less than the nominal displacement of the piezoelectric actuators, i.e. the displacement under free condition. It is demonstrated that the stiffness of the preload mechanism has a significant effect on the performance of the piezo-driven mechanism.

The displacement of the end-effector for the two piezoelectric actuator driving is shown in Fig.11. Both the FEA and experimental results are provided. The analytical results are also obtained based on the developed kinematic model. It is noted that the FEA results are in good agreement with the experimental results, but a little bit difference with the analytical results. The main reason for the difference is that the flexure hinge is not the ideal revolute pivot, and the rotational center of the flexure hinge will drift during the motion of the connected links. Thus, the actual displacement of the end-effector and the amplification factor of the developed mechanism are little difference from the theoretical ones.

Conclusions

The design methodology of a five-bar compliant mechanism with lever mechanisms has been described, and the prototype of the compliant micro-manipulator has been designed and constructed. From the kinematic point of view, the entire compliant micro-manipulator has

been divided into a five-bar mechanism and two four-bar amplification mechanisms. The amplification factor has been obtained by considering the lever mechanism as a special four-bar linkage.

The forward kinematics for the Cartesian displacement and velocity of the five-bar compliant micro-manipulator has been obtained by solving the intersection of the two circles with the centers located at the end of the active links and the radii equal to the length of passive links. Accordingly, the Cartesian coordinates of the end-effector attached to one of the passive links is obtained based on the geometric relationship. The local mobility index of the five-bar compliant mechanism has been established and analyzed.

Based on the simplified methodologies such as linearising the trigonometric functions and constant Jacobian matrix, different approaches for the forward kinematics have been proposed and the performance of the five-bar compliant manipulator is investigated. The comparisons between the exact solutions and simplified methods were carried out. It is noted that the linearization of trigonometric functions has a higher accuracy and is more suitable for the kinematic calculation of the micro-manipulator, but the constant Jacobian matrix method can efficiently calculate the forward kinematics of the micro-manipulator with the acceptable accuracy and is the optimal choice for the real-time control system.

Both FEA and experimental tests are carried out to verify the established model and the performance of the proposed five-bar mechanism. The considerable coincidence shows that the developed model for the kinematic analysis is correct, and the lever mechanisms can implement the function of displacement amplification. It must be pointed out that the actual amplification factor is approximately 80 percent of the nominal value which is set as 2. This

is mainly due to the offset of the flexure hinges. Thus, more efforts should be directed to this issue during the flexure-based mechanism design to achieve the desirable performance.

Acknowledgment

This research is supported by the Australian Research Council (ARC) Discovery (grant Nos. DP 0668052, DP0986814), ARC Linkage Infrastructure, Equipment and Facilities (grant Nos. LE0347024, LE0668508), and National Natural Science Foundation of China (grant No. 50705064).

References

[1] Q. Yao, J. Dong, and P. M. Ferreira, "Design, analysis, fabrication and testing of a parallel-kinematic micropositioning XY stage," International Journal of Machine Tools and Manufacture, vol. 47, no. 6, pp. 946-961, May 2007.

[2] S.T. Smith, D.G. Chetwynd, D.K. Bowen, "Design and assessment of monolithic high precision translation mechanisms," Journal of Physics E: Science Instrument, vol. 20, no. 8, pp. 977-983, August 1987.

[3] J. A. Miller, R. Hocken, S. T. Smith, and S. Harb, "X-ray calibrated tunneling system utilizing a dimensionally stable nanometer positioner," Precision Engineering, vol. 18, no. 2-3, pp. 95-102, April 1996.

[4] Y. Tian, X. Liu, D. Zhang, and D.G. Chetwynd, "Dynamic modeling of the fidelity of random surface measurement by the stylus method," Wear (2008), doi:10.1016/j.wear.2008.04.061.

[5] K. B. Choi and J. J. Lee, "Passive compliant wafer stage for single-step nano-imprint lithography," Review of Scientific Instruments, vol. 76, no. 5, pp. 075106, May 2005.

[6] G. Alici and B. Shirinzadeh, "Enhanced stiffness modeling identification and characterization for robot manipulators," IEEE Transactions on Robotics, vol. 21 no. 4, pp. 554-564, August 2005.

[7] O. Nakamura, M. Goto, and K. Toyoda, “Laser tracking robot performance calibration system using ball-seated bearing mechanisms and a spherically shaped cat’s eye retroreflector,” Review of Scientific Instruments, vol. 65, no. 4, pp. 1006-1011, April 1994.

[8] G. Alici and B. Shirinzadeh, “A systematic technique to estimate positioning errors for robot accuracy improvement using laser interferometry based sensing,” Mechanism and Machine Theory, vol. 40, no. 8, pp. 879-906, August 2005.

[9] P. L. Teoh, B. Shirinzadeh, C. W. Foong, and G. Alici, “The measurement uncertainties in the laser interferometry-based sensing and tracking technique,” Measurement, vol. 32, no. 2, pp. 135-150 , September 2002.

[10] Y. Tian, B. Shirinzadeh, D. Zhang, and G. Alici, “Development and dynamic modelling of a flexure-based Scott-Russell mechanism for nano-manipulation,” Mechanical Systems and Signal Processing (2008), doi:10.1016/j.ymssp.2008.06. 007.

[11] B. Shirinzadeh, P. L. Teoh, Y. Tian, M. M. Dalvand, Y. Zhong, and H. C. Liaw, “Laser interferometry-based guidance methodology for high precision positioning of mechanisms and robots,” Robotics and Computer-Integrated Manufacturing, submitted for publication.

[12] J. J. Craig, Introduction to Robotics: Mechanics and Control, 3rd ed. Upper Saddle River, New Jersey: Pearson, 2005.

[13] J. M. Paros and L. Weisbord, “How to design flexure hinges,” Machine Design, vol. 37, pp. 151-156, November 1965.

[14] D. Zhang, D. G. Chetwynd, X. Liu, and Y. Tian, “Investigation of a 3-DOF micro-positioning table for surface grinding,” International Journal of Mechanical Sciences, vol. 48, no. 12, pp. 1401-1408, December, 2006.

[15] N. Lobontiu and J. S. N. Paine, “Design of circular cross-section corner-filleted flexure hinges for three-dimensional compliant,” Journal of Mechanical Design, Transactions of ASME, vol. 124, no. 3, pp. 479- 484, September 2002.

[16] S. T. Smith, V. G. Badami, J. S. Dale, and Y. Xu, "Elliptical flexure hinges," Review of Scientific Instruments, vol. 68, no. 3, pp. 1474- 1483, March 1997.

[17] A. T. Elfizy, G. M. Bone, and M. A. Elbestawi, "Design and control of a dual-stage feed drive," International Journal of Machine Tools and Manufacture, vol. 45, no. 2, pp. 153-165, February 2005.

[18] Y. Gao, D. W. Zhang, and C. W. Yu, "Dynamic modeling of a novel workpiece table for active surface grinding control," International Journal of Machine Tools and Manufacture, vol. 41, no. 4, pp. 609- 624, March 2001.

[19] J. L. Stephen, A. C. David, and A. C. Joseph, "Design of a rotary fast tool servo for ophthalmic lens fabrication," Precision Engineering, vol. 23, no. 4, pp. 253-259, October 1999.

[20] J. Speich and M. Goldfarb, "A compliant mechanism based three degree of freedom manipulator for small-scale manipulation," Robotica, vol. 18, no. 1, pp. 95-104, January 2000.

[21] M. L. Culpepper and G. Anderson, "Design of a low-cost nano-manipulator which utilizes a monolithic, spatial compliant mechanism," Precision Engineering, vol. 28, no. 4, pp. 469-489, October 2004.

[22] P. Gao and S. M. Swei, "A six-degree-of-freedom micro-manipulator based on piezoelectric translators," Nanotechnology, vol. 10, no. 4, pp. 447-452, December 1999.

[23] A. M. Dollar and R. D. Howe, " A robust compliant grasper via shape deposition manufacturing," IEEE/ASME Transactions on Mechatronics, vol. 11, no. 2, pp. 154-161, April 2006.

[24] Y. M. Li and Q. S. Xu, "A novel design and analysis of a 2-DOF compliant parallel micromanipulator for nanomanipulation," IEEE Transactions on Automation Science and Engineering, vol. 3, no. 3, pp. 248-254, July 2006.

[25] H. C. Liaw, B. Shirinzadeh, and J. Smith, "Enhanced sliding mode motion tracking control of actuators," Sensors and Actuators A: Physical, vol. 138, no. 1, pp. 194-202, July 2007.

[26] Y.M. Tseytlin, "Notch flexure hinges: An effective theory," Review of Scientific Instruments, vol. 73, no. 9, pp. 3363-3368, September 2002.

[27] N. Lobontiu, J. S. N. Paine, E. O'Malley, and M. Samuelson, "Parabolic and hyperbolic flexure hinges: flexibility, motion precision and stress characterization based on compliance closed-form equations," Precision Engineering, vol. 26, no. 2, pp.183-192, February 2002.

[28] H. C. Liaw, B. Shirinzadeh, and J. Smith, "Robust motion tracking control of piezo-driven flexure-based four-bar mechanism for micro/ nano manipulation," Mechatronics, Vol.18, no.2, pp.111-120, March, 2008.

[29] Y. Tian, B. Shirinzadeh and D. Zhang, "A flexure-based mechanism and control methodology for ultra-precision turning operation," Precision Engineering, doi: 10.1016/j.precisioneng. 2008.05. 001.

[30] W. J. Zhang, J. Zou, L. G. Waston, W. Zhao, G. H. Zong, and S. S. Bi, "The constant-jacobian method for kinematics of three-DOF planar micro-motion stage," Journal of Robotic Systems, vol. 19, no. 2, pp. 63-72, February 2002.

List of figure captions

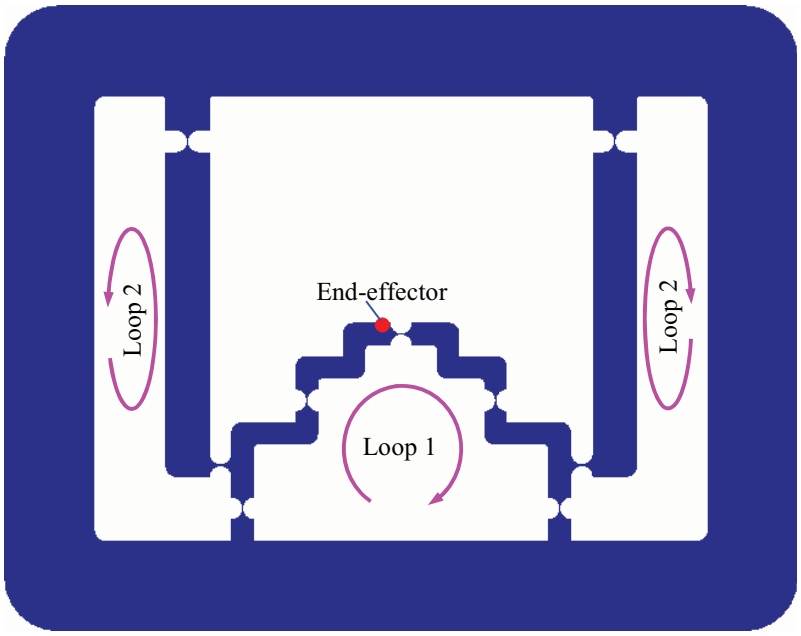

Fig.1. Geometric model of the five-bar micro-manipulator

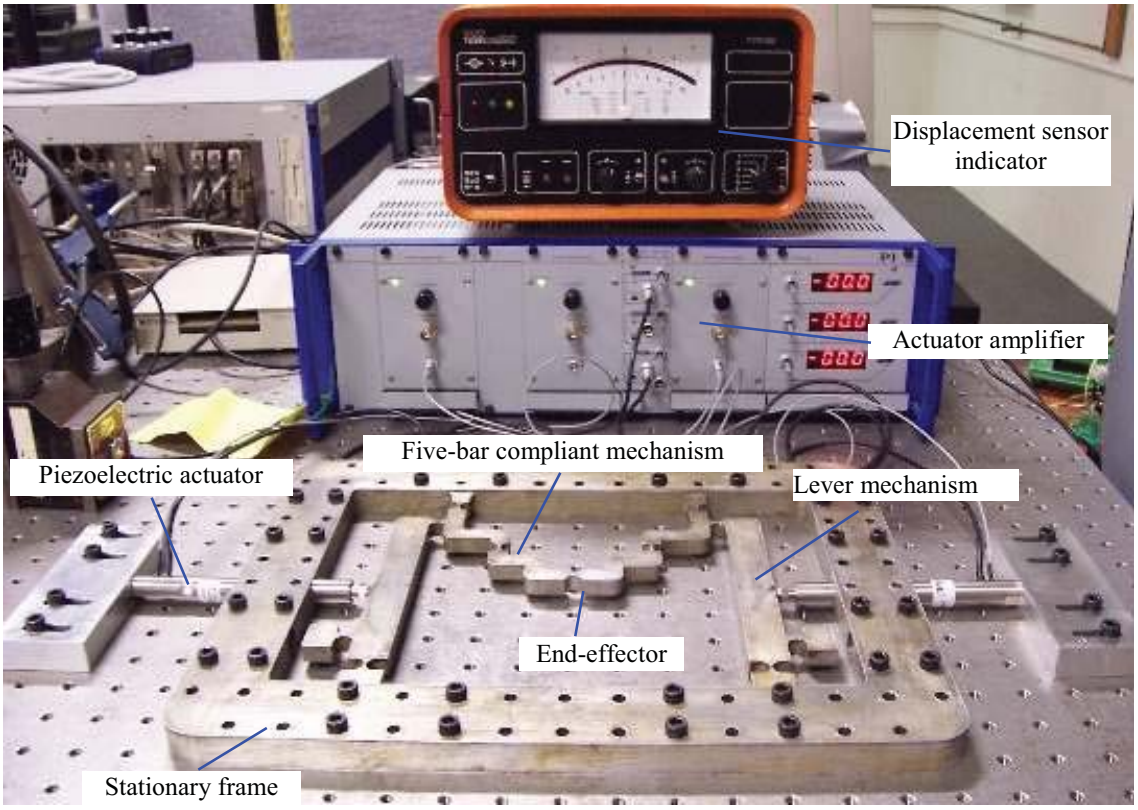

Fig.2. Photo of the five-bar micro-manipulator

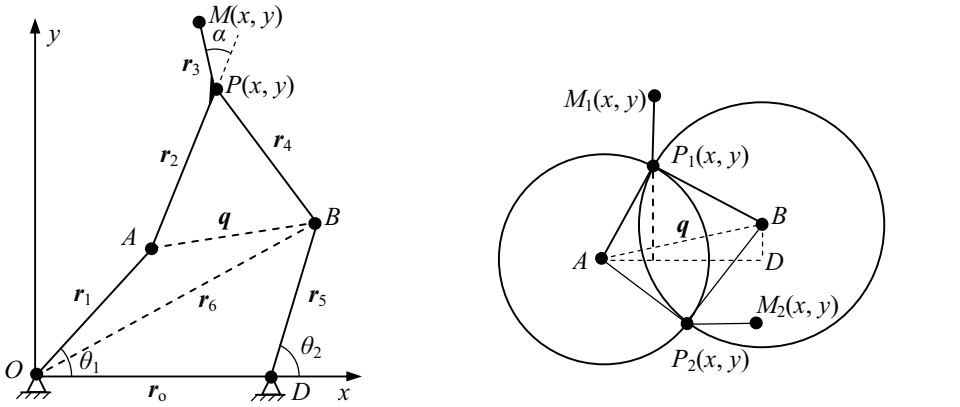

(a) Geometric model (b) Description of the position of point P

Fig.3. Kinematic model of the five-bar mechanism

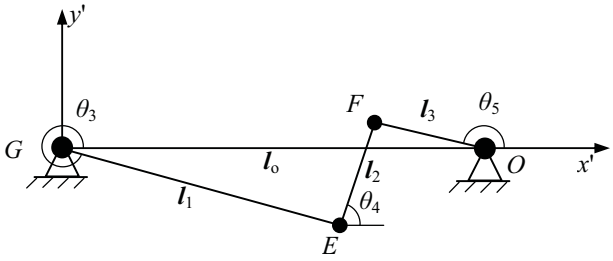

Fig.4. Kinematic model of the lever mechanism

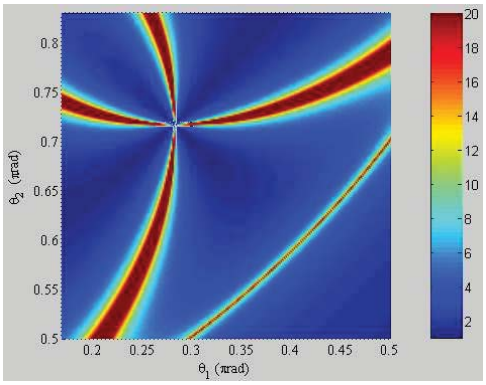

(a) Point P

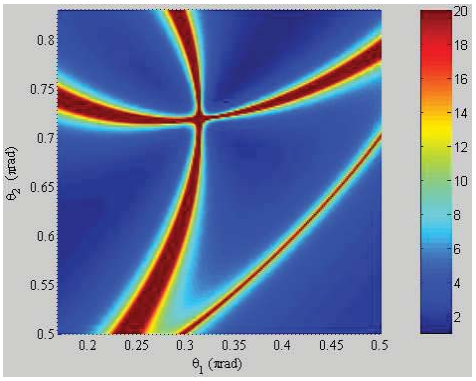

(b) Point M (α=π/3, r_3=15)

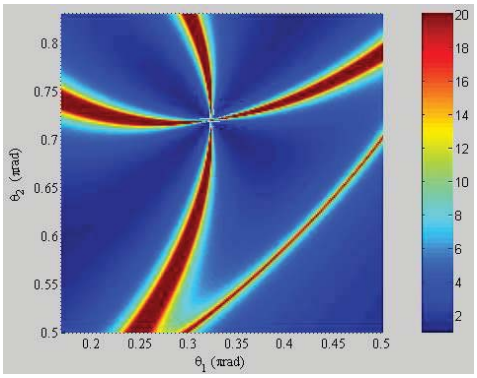

(c) Point M (α=π/2, r_3=15)

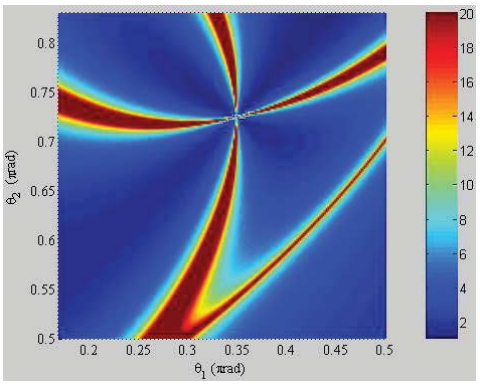

(d) Point M (α=π/2, r_3=25)

Fig.5. Local mobility index of the different end-effectors

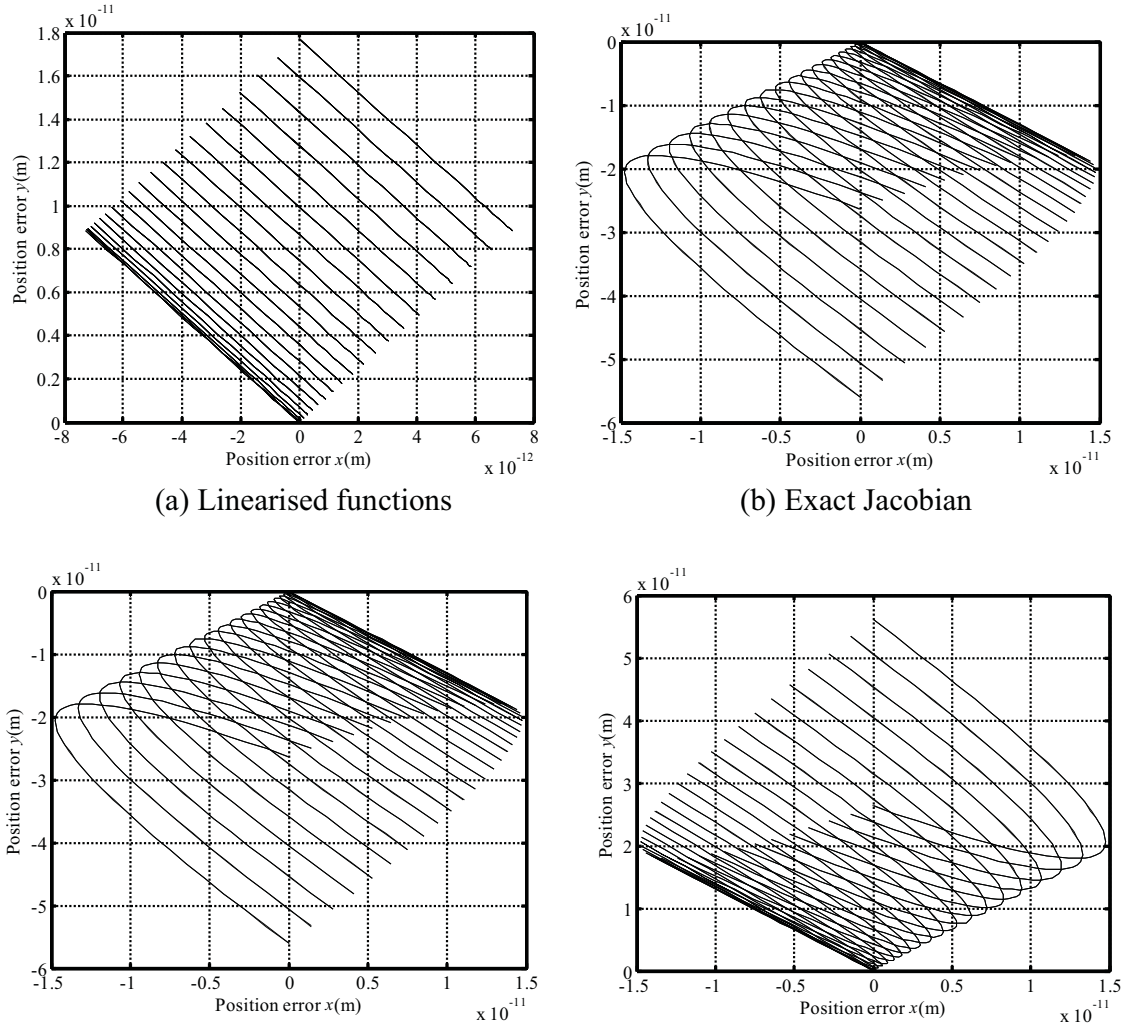

(a) Linearised functions (b) Exact Jacobian

(c) Linearised Jacobian (d) Constant Jacobian

Fig.6. Position errors of the point P in x and y directions

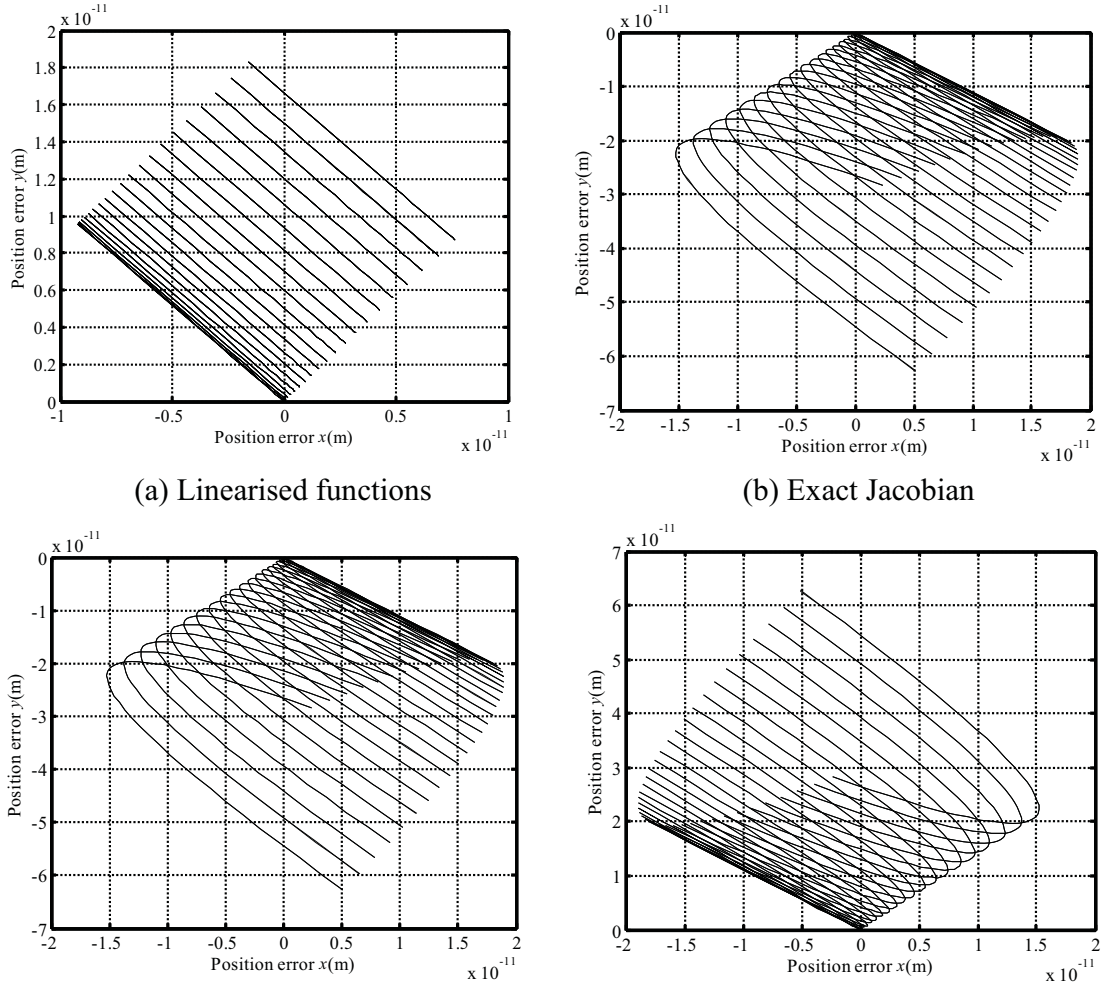

(a) Linearised functions (b) Exact Jacobian

(c) Linearised Jacobian (d) Constant Jacobian

Fig.7. Position errors of the point *M* in *x* and *y* directions

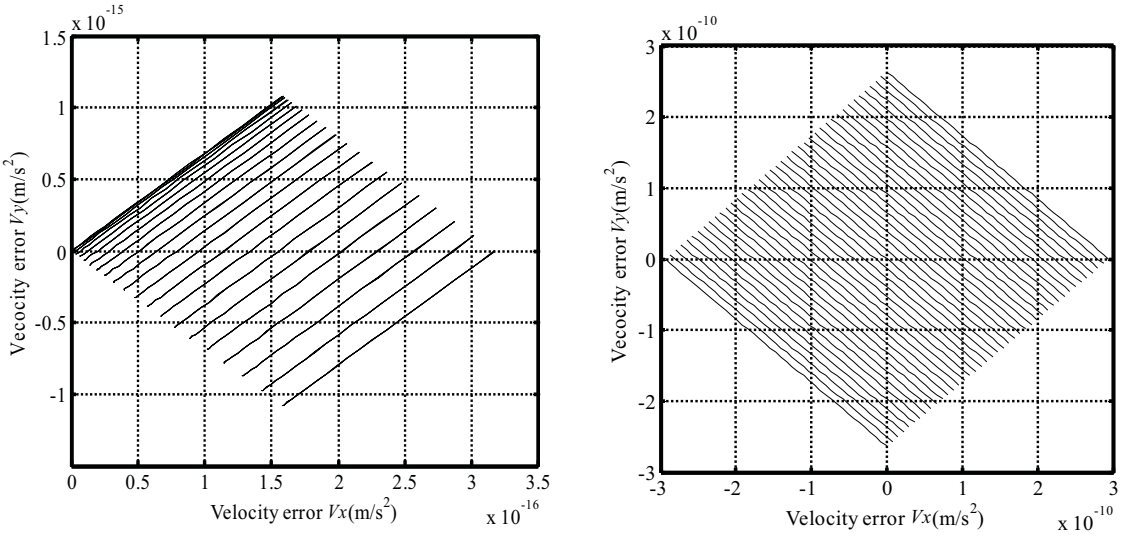

(a) Linearised Jacobian (b) Constant Jacobian

Fig.8. Velocity errors of the point *P* in *x* and *y* directions

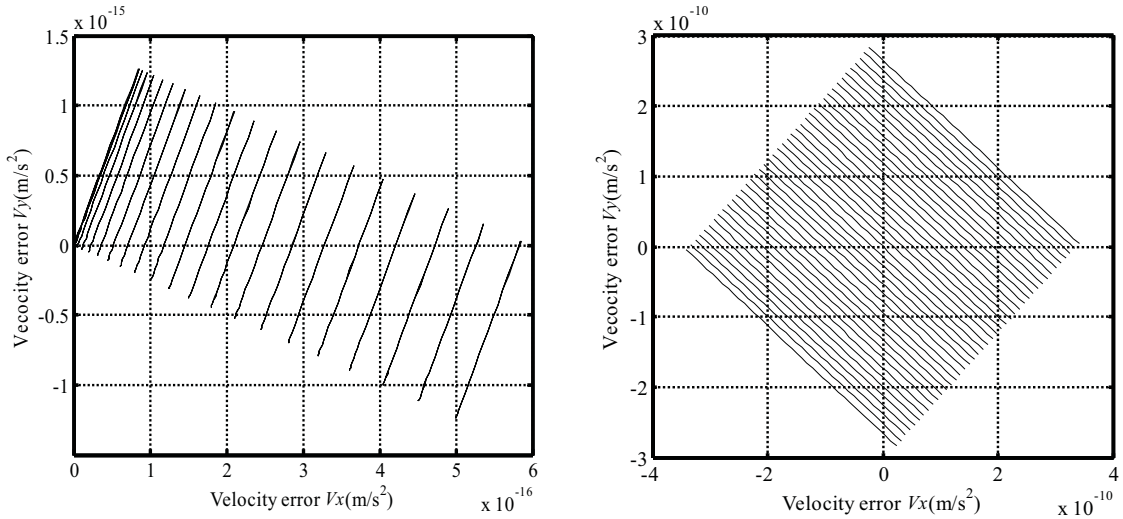

(a) Linearised Jacobian (b) Constant Jacobian

Fig.9. Velocity errors of the point *M* in *x* and *y* directions

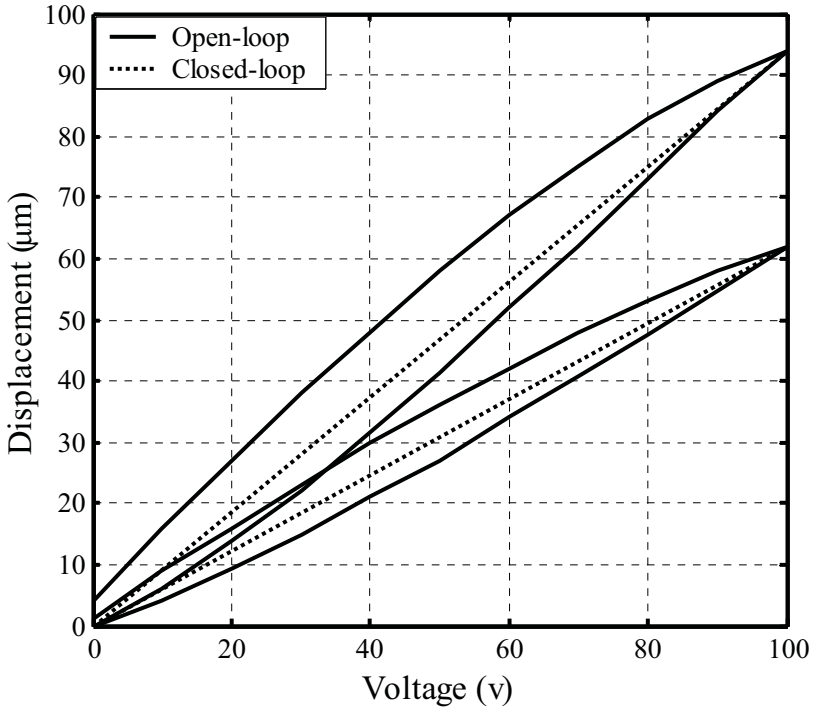

(a) Left driving piezoelectric actuator

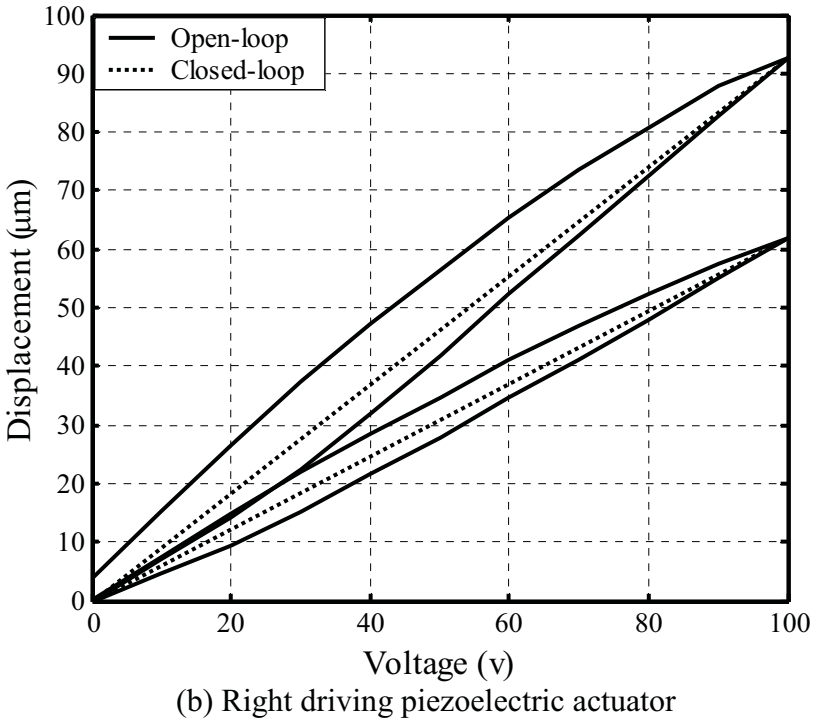

(b) Right driving piezoelectric actuator

Fig.10. Displacement characteristics of the piezoelectric actuators

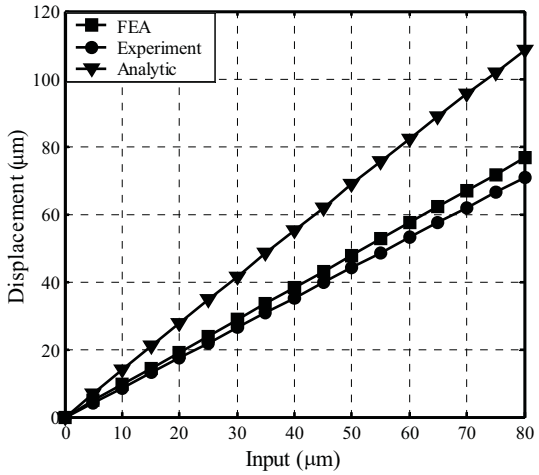

(a) Displacement in *x*-direction driven by left actuator

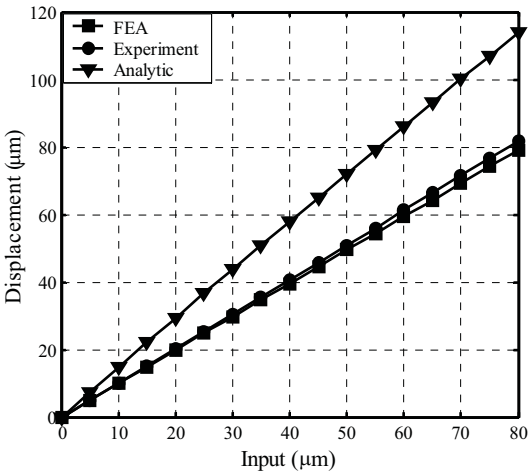

(b) Displacement in *y*-direction driven by left actuator

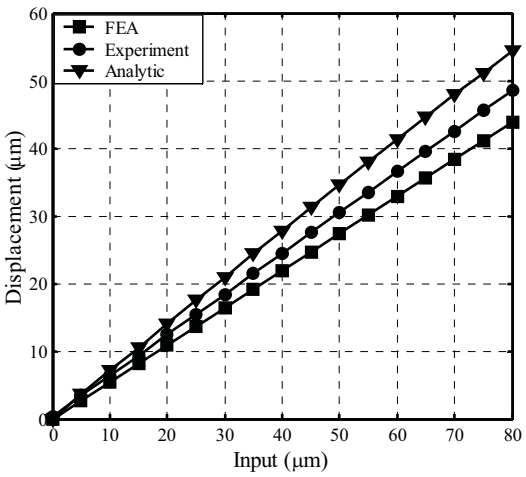

(c) Displacement in *x*-direction driven by right actuator

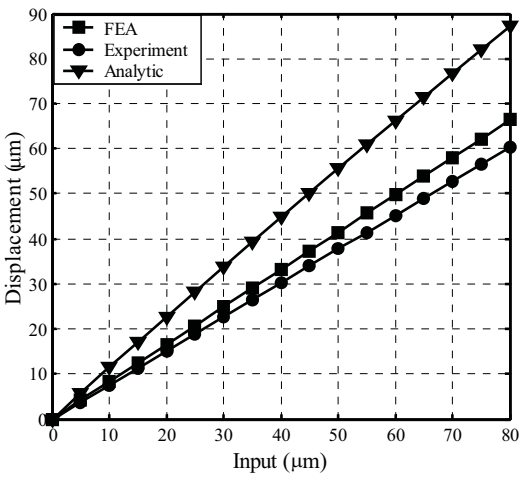

(d) Displacement in *y*-direction driven by right actuator

Fig.11. Displacement of the flexure-based micro-manipulator